The realization of long-wavelength (λ ≤ 2.3 μm) $Ga_{1-x}In_xAs_{1-y}N_y$ quantum wells on InP by molecular-beam epitaxy

2004 J. Phys.: Condens. Matter 16 S2995

(http://iopscience.iop.org/0953-8984/16/31/001)

INSTITUTE OF PHYSICS PUBLISHING JOURNAL OF PHYSICS: CONDENSED MATTER

J. Phys.: Condens. Matter **16** (2004) S2995–S3008 PII: S0953-8984(04)75529-0

The realization of long-wavelength ($\lambda \leqslant 2.3\ \mu$m) $Ga_{1-x}In_xAs_{1-y}N_y$ quantum wells on InP by molecular-beam epitaxy

K Köhler, J Wagner, P Ganser, D Serries[1], T Geppert[2], M Maier and L Kirste

Fraunhofer-Institut für Angewandte Festkörperphysik, Tullastrasse 72, D-79108 Freiburg, Germany

Received 23 January 2004
Published 23 July 2004
Online at stacks.iop.org/JPhysCM/16/S2995
doi:10.1088/0953-8984/16/31/001

Abstract

The epitaxial growth and characterization of dilute $Ga_{1-x}In_xAs_{1-y}N_y$ films and quantum wells are presented. Starting with the epitaxy on GaAs, recent results on the local bonding of nitrogen in $Ga_{1-x}In_xAs_{1-y}N_y$ are reviewed, revealing that bonding of nitrogen is controlled by an interplay between bond cohesive energy and reduction of local strain. Thus, III–N bonding in $Ga_{1-x}In_xAs_{1-y}N_y$ can be changed from Ga–N to In–N by post-growth thermal annealing. Nitrogen loss due to the annealing process is not observed. We then adopted this concept for the epitaxy on InP substrates, which is equivalent to a drastic increase in indium content of the $Ga_{1-x}In_xAs_{1-y}N_y$ system and thus an extension to longer wavelengths. The low-energy shift of quaternary pseudomorphically strained $Ga_{0.4}In_{0.6}As_{1-y}N_y$ double quantum wells upon nitrogen incorporation is reported. The deterioration of the photoluminescence characteristics in terms of reduced peak intensity and increased linewidth with increasing nitrogen incorporation can be partially compensated by rapid thermal annealing, which is accompanied by a blueshift with respect to the as-grown samples. Within the resolution limits of our secondary ion mass spectrometry experiments, no annealing-induced loss of nitrogen was observed even for the high indium content $Ga_{1-x}In_xAs_{1-y}N_y$ quantum well structures. The results on indium-rich highly strained $Ga_{0.22}In_{0.78}As_{0.99}N_{0.01}$ quantum wells on InP substrate are reported, showing room temperature photoluminescence at wavelengths up to 2.3 μm. We finally conclude with the demonstration of multi quantum well lasers emitting at wavelengths beyond 2 μm.

(Some figures in this article are in colour only in the electronic version)

[1] Present address: Adam Opel AG, Rüsselsheim, Germany.
[2] Present address: Max Planck Institut für Mikrostrukturphysik, 06120 Halle, Germany.

1. Introduction

The $GaAs_{1-y}N_y$ and $Ga_{1-x}In_xAs_{1-y}N_y$ alloy systems with N concentrations in the range of a few per cent are of considerable technological interest, allowing the realization of long-wavelength photodetectors and laser diodes on GaAs substrates [1–3]. The fundamental physical properties of these alloys are, however, equally interesting and intriguing. Substitution of arsenic atoms by the much smaller N atoms, their atomic radius being 40% smaller, with very different chemical properties, leads to material properties deviating greatly from those expected for a conventional alloy. Replacing a few per cent of As by N in GaAs or $Ga_{1-x}In_xAs$ results in a significant reduction of the fundamental bandgap energies [4, 5], even though the bandgap of GaN is much larger than that of GaAs [6]. In addition, N compensates the compressive strain introduced by the incorporation of In.

These properties enable long-wavelength emitters to be realized on GaAs substrate. Consequently most of the research has concentrated so far on the successful development of 1.3 μm diode lasers on GaAs substrate for applications in fibre-optic communication [7, 8]. In contrast to the large amount of work reported on dilute $Ga_{1-x}In_xAs_{1-y}N_y$ on GaAs [9], only a few studies have been published so far on high In content (beyond 53%) $Ga_{1-x}In_xAs_{1-y}N_y$ on InP [10–13]. These studies showed both experimentally [10, 12, 13] as well as theoretically [11] that, similar to dilute $Ga_{1-x}In_xAs_{1-y}N_y$ on GaAs, the addition of N to lattice matched or compressively strained $Ga_{1-x}In_xAs$ on InP results in a sizeable reduction of the bandgap energy of the resulting InP-based $Ga_{1-x}In_xAs_{1-y}N_y$ layer, accompanied by a reduction in the lattice constant. Thus, the concept employed to reach wavelengths $\geqslant 1.3$ μm on GaAs, which is to use $Ga_{1-x}In_xAs_{1-y}N_y$ QWs with In contents above the limit for relaxation of pseudomorphic strain in ternary $Ga_{1-x}In_xAs$, in conjunction with typically 1–2% N to compensate the excess strain plus additionally lowering the gap energy, can also be applied to achieve long-wavelength ($\lambda \geqslant 2.3$ μm) emission QWs on InP.

Shan *et al* [14, 15] proposed the band anticrossing (BAC) model to describe the composition dependence of the bandgap energy of dilute $Ga_{1-x}In_xAs_{1-y}N_y$ on GaAs. This model is based on the interaction of the lowest conduction band with the highly localized N-induced energy level E_N, located 1.64 eV above the valence band edge of GaAs. Starting from GaAs, figure 1 shows the bandgap energies of the ternary alloys $GaAs_{1-y}N_y$ (dashed curve, calculated using the interaction parameter $C_{MN} = 2.7$ eV [15]) and $Ga_{1-x}In_xAs$ (solid line) as functions of the lattice parameters. In this paper we concentrate on dilute $Ga_{1-x}In_xAs_{1-y}N_y$ on InP substrate as an extension of the $Ga_{1-x}In_xAs_{1-y}N_y$ on GaAs system. Thus in figure 1 the bandgap energy versus lattice parameter relation is also plotted for $Ga_{0.22}In_{0.78}As_{1-y}N_y$ (bold solid curve). The composition is chosen deliberately as our laser structures are grown with that Ga to In concentration ratio. The curve is calculated from the BAC model [14, 15] using the interaction parameter $C_{MN} = 2.3$ eV for $Ga_{0.22}In_{0.78}As_{1-y}N_y$. The interaction parameter is an average value for high In-containing samples taken from Serries *et al* [13].

This paper is organized as follows. Section 2 describes the growth of the samples investigated and the experimental techniques used for sample characterization, including necessary calibrations. Results are presented and discussed in section 3, which is divided in four parts. First, we briefly discuss selected results obtained for $Ga_{1-x}In_xAs_{1-y}N_y$ on GaAs, which we consider to be a reference necessary for the understanding of the following results derived for high In-containing $Ga_{1-x}In_xAs_{1-y}N_y$ on InP. We then concentrate on $Ga_{0.4}In_{0.6}As_{1-y}N_y$ on InP in its as-grown state in the second part, and post-growth annealed in the third part. The fourth part of section 3 is dedicated to first results on long-wavelength $Ga_{1-x}In_xAs_{1-y}N_y$ quantum well laser structures on InP. Finally, section 4 concludes this work.

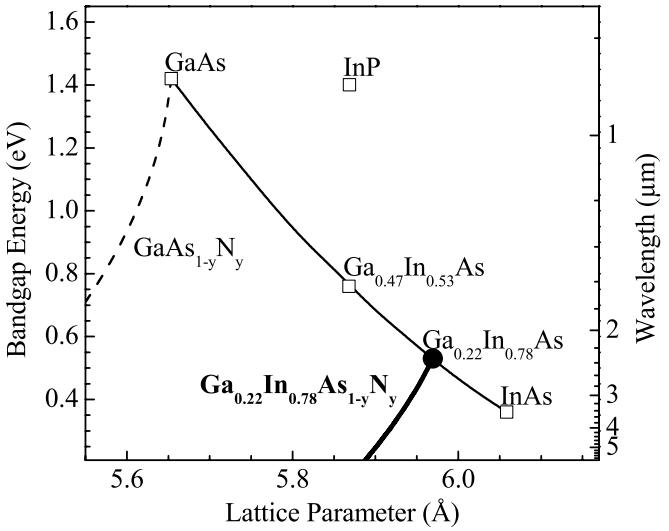

Figure 1. Bandgap energy versus lattice parameter of $GaAs_{1-y}N_y$ (C_{MN} = 2.7 eV [15]), $Ga_{1-x}In_xAs$ and $Ga_{0.22}In_{0.78}As_{1-y}N_y$, calculated within the framework of the BAC-model [14, 15]. An averaged interaction parameter (C_{MN} = 2.3 eV) for $Ga_{0.22}In_{0.78}As_{1-y}N_y$ was taken from [13].

2. Growth and experimental details

Quaternary $Ga_{1-x}In_xAs_{1-y}N_y$ on (001)GaAs and $Ga_{1-x}In_xAs_{1-y}N_y$ on (001)InP layers as well as $Ga_{1-x}In_xAs_{1-y}N_y/Al_{0.48}In_{0.52}As$ on (001)InP QWs were grown in a Varian Gen II Modular molecular-beam epitaxy (MBE) system using Al, Ga, In and As solid sources and an rf nitrogen plasma source. The growth rate was about 1.5 μm h^{-1}. The optimum growth temperature, which is dependent on the In content of the structure, was in the range of 530–580 °C on GaAs and 490–550 °C on InP. Laser structures were grown on sulfur (3–6) $\times 10^{18}$ cm^{-3} doped InP by MBE in combination with low pressure metal-organic vapour-phase epitaxy (MOVPE). The whole active region was grown by MBE while low pressure (100 mbar) MOVPE was used for the overgrowth with the upper p-doped InP cladding layer. For the MOVPE growth PH_3, AsH_3, TMIn, and TMGa were used as precursors. The growth rate was about 2 μm h^{-1}, and the growth temperature was 560 °C. Post-growth rapid thermal annealing (RTA) was performed on SiON encapsulated pieces of selected wafers in an N_2 ambient for 20 or 60 s and at various temperatures between 650 and 950 °C.

Coherently strained 50–200 nm thick III–AsN layers, grown on either (001)GaAs or InP substrates, and InP-based $Ga_{1-x}In_xAs_{1-y}N_y/Al_{0.48}In_{0.52}As$ QWs were analysed by high-resolution x-ray diffraction (HRXRD) and secondary ion mass spectrometry (SIMS) to determine the strain state as well as the chemical composition. Cs primary ions with an energy of 1 keV and at an angle of incidence of 45° were used for depth profiling. The SIMS measurements were calibrated using appropriate standards prepared by implantation of nitrogen at an energy of 75 keV and a dose of 5 $\times$ 10^{15} N_2 molecules cm^{-2} into $Ga_{1-x}In_xAs$ with compositions spanning the range between GaAs and InAs [16].

Photoluminescence (PL) measurements on $Ga_{1-x}In_xAs_{1-y}N_y$ on InP layers as well as InP-based $Ga_{1-x}In_xAs_{1-y}N_y/Al_{0.48}In_{0.52}As$ QWs were performed at low temperature (10 K) as well as at room temperature (300 K), using an Nd^{3+}–YAG laser emitting at 1.064 μm (1.16 eV) for excitation and a Fourier-transform infrared (FTIR) spectrometer for detection of

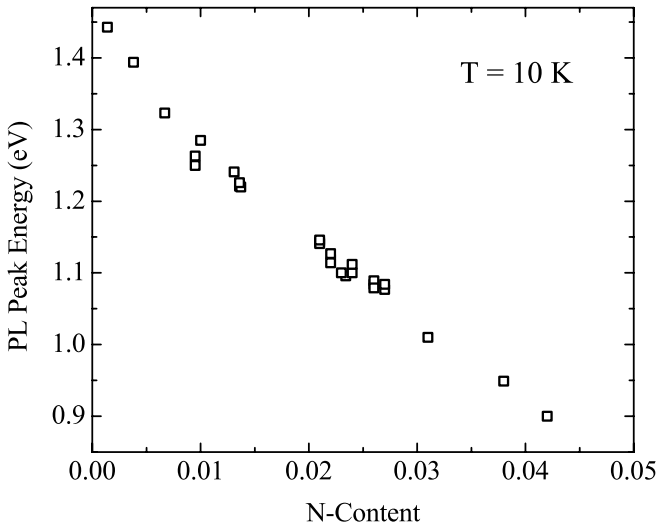

Figure 2. The low-temperature (10 K) PL peak position of 100–150 nm $GaAs_{1-y}N_y$ films on GaAs versus N content determined by HRXRD.

the luminescence signal. Raman spectra from GaAs-based III–AsN layers were recorded in backscattering geometry from the (001) growth surface. To maximize the intensity of Raman scattering from N-induced vibrational modes, the 568.2 nm (2.18 eV) line of a Kr-ion laser was used for optical excitation close to resonance with the mostly N-derived E_+ transition [17–19]. Incident and scattered light were polarized parallel to the same (110)-type crystallographic direction ($x(y', y')$–x scattering configuration).

3. Results and discussion

3.1. Results on GaAs

Strained ternary $GaAs_{1-y}N_y$ films with layer thicknesses of 100–150 nm and N content from 0.4% up to 4.2% were used as a starting point before switching to quaternary $Ga_{1-x}In_xAs_{1-y}N_y$/GaAs heterostructures. The N content of the GaAs layers was calculated, based on Vegard's rule, from the lattice mismatch as determined by HRXRD. SIMS analysis was used for an independent determination of the N content. The PL spectra of these samples showed a redshift in energy down to 0.9 eV for an N content of 4.2%, as can be seen in figure 2, in agreement with previous reports, e.g. [20]. To determine the interaction parameter C_{MN} [14, 15] the PL results of the layers have to be corrected with respect to tensile strain, and an offset of 35 meV was assumed for the difference between the bandgap energy and the energy position of the maximum in the near band edge PL spectrum. This results in a C_{MN} of 2.7 eV in agreement with Shan *et al* [15].

The effect of RTA was tested on a 50 nm $GaAs_{1-y}N_y$ film with high N content; the annealing temperature was 850 °C for 60 s. Figure 3 shows the SIMS profiles of the ternary film with (solid curve) and without RTA (bold curve). There is no detectable loss of N, and no diffusion or broadening. SIMS yields 4.6% of N for the as-grown sample and 4.5% for the RTA sample, which is a relative difference of as little as 2%, which is clearly within the reproducibility limit of 5% for the SIMS measurement. HRXRD on the same samples yields concentrations of 5.2 ± 0.2% for the as-grown sample and 4.9 ± 0.2% for the RTA sample, supporting the above result. However, we do observe a blueshift in the PL spectra of the thermally annealed samples of 20–40 meV, dependent on the growth temperature of the

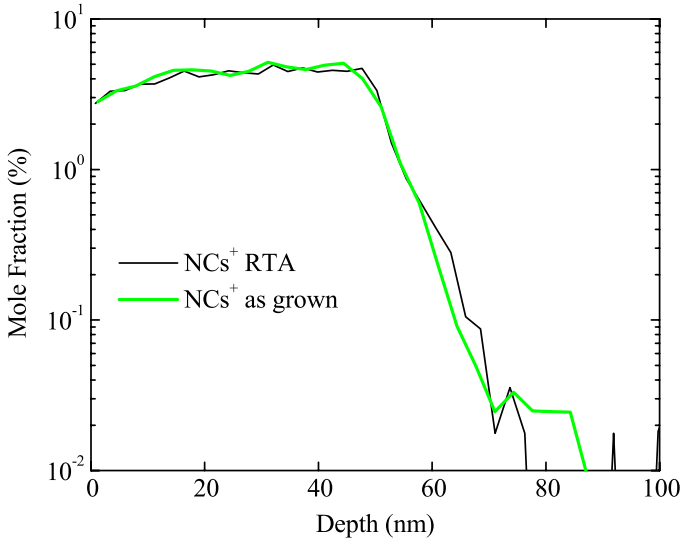

Figure 3. SIMS depth profile of a 50 nm thick $GaAs_{0.96}N_{0.04}$ layer as-grown (bold curve) and after rapid thermal annealing at 850 °C for 60 s (full curve).

$GaAs_{1-y}N_y$. Increasing the growth temperature by 60 °C yields 20 meV. This effect is also seen by Buyanova *et al* [21]. The RTA induced high-energy shift observed for samples grown at higher temperature has been interpreted as an improvement of the alloy uniformity [21].

In low N content $GaAs_{1-y}N_y$ a single N-related vibrational mode is observed at around 470 cm^{-1}, as shown in figure 4. There, room temperature and low-temperature (77 K) Raman spectra are plotted for a $GaAs_{0.99}N_{0.01}$ layer, showing clearly the GaN-like LO_2 mode, which is particularly well resolved in the 77 K spectrum. This mode has been assigned to the vibration of an isolated N atom, bonded to four Ga neighbours [22]. On adding In to $GaAs_{1-y}N_y$, i.e. forming the quaternary compound $Ga_{1-x}In_xAs_{1-y}N_y$, two additional modes appear at the high- and low-frequency side of the GaN-like LO_2 mode, as can be seen from figure 5. These modes have been assigned to the vibration of N bonded to at least one In neighbour [18, 23, 24]. Both InN-like modes gain strength upon rapid thermal annealing at 850 °C for 60 s at the expense of the GaN-like mode intensity, which is evident from a comparison of the spectra recorded from as-grown and annealed $Ga_{0.93}In_{0.07}As_{0.98}N_{0.02}$ displayed in figure 5. This annealing-induced change in N bonding towards more In–N bonds has been explained by an interplay between the larger cohesive energy [25] of the Ga–N bond of 2.24 eV as compared to the In–N bond (1.93 eV), and reduced local strain energy [26] when In–N bonds are formed [24]. At the growth surface N incorporation is controlled by the bond cohesive energy, favouring the formation of Ga–N bonds. In the bulk of the material, in contrast, N surrounded by four Ga neighbours introduces considerable local strain due to the short Ga–N bond length. This strain can be reduced by introducing In–N bonds with a larger bond length, making the formation of, for example, Ga_3InN complexes more favourable in spite of the lower In–N bond cohesive energy [27]. Thus, upon annealing, the fraction of In–N bonds is expected to increase, as is observed experimentally.

3.2. Growth on InP

The effect of N incorporation on the $Ga_{1-x}In_xAs_{1-y}N_y$ lattice parameter along the growth axis, and thus the in-plane biaxial strain, is illustrated in figure 6. There, HRXRD radial scans around the InP 004 reflection are shown for a 165 nm thick pseudomorphic $Ga_{0.41}In_{0.59}As_{0.983}N_{0.017}$ layer and, for comparison, of a $Ga_{0.41}In_{0.59}As$ reference sample of equal thickness; the two

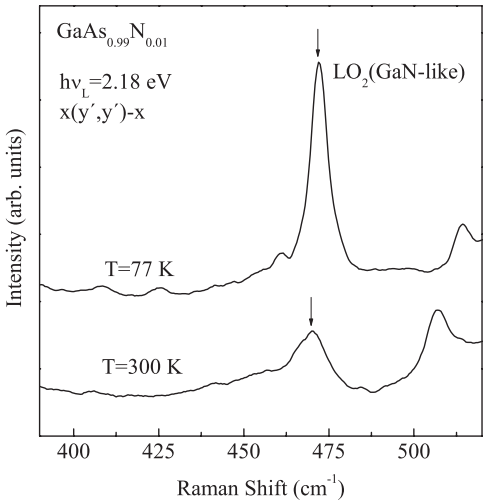

Figure 4. Raman spectra of $GaAs_{0.99}N_{0.01}$ on GaAs recorded at 77 K (upper spectrum) and 300 K (lower spectrum).

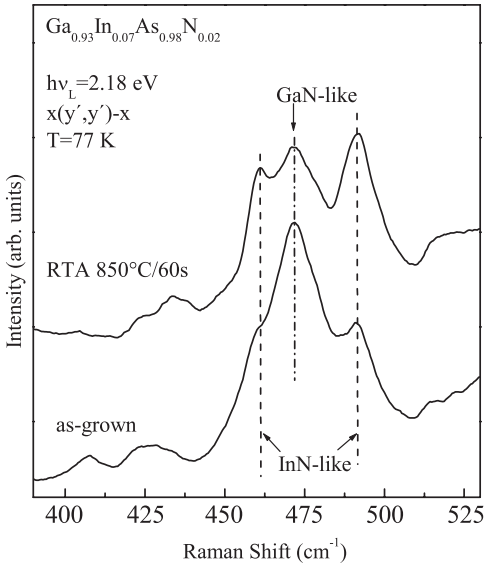

Figure 5. Low-temperature (77 K) Raman spectra of as-grown (bottom) and rapid thermal annealed $Ga_{0.93}In_{0.07}As_{0.98}N_{0.02}$ on GaAs (top).

samples were prepared in successive growth runs. The incorporation of N leads to a clear reduction of the compressive pseudomorphic strain from $\Delta d/d = +8.6 \times 10^{-3}$ to $+1.9 \times 10^{-3}$, as can be seen from the shift of the $Ga_{1-x}In_xAs_{1-y}N_y$ 004 diffraction peak to larger diffraction angles. Extended bond method HRXRD [28] measurements confirmed that both layers were fully strained to the in-plane lattice parameter of the InP substrate. For the ternary layer the In content was 59% as determined from the HRXRD profile. The In content of the quaternary film was assumed to be identical to that of the ternary reference sample. This assumption was verified by SIMS measurements, showing that the incorporation of In even at such high concentrations was not affected by the presence of N in the $Ga_{1-x}In_xAs_{1-y}N_y$ sample. The reduction in strain for the quaternary sample can thus be exclusively attributed to the incorporation of 1.7% N, assuming Vegard's rule to be valid. SIMS measurements detecting NCs^+ ions yielded an N content of 1.5%. Within the accuracy limits of these two experimental techniques both results are in good agreement.

Low-temperature PL measurements at 10 K are shown in figure 7. The PL peak position of the ternary sample was at 0.75 eV, and the full width at half maximum (FWHM) was 6.7 meV. Upon incorporating 1.7% of N the PL peak position was redshifted to 0.61 eV, i.e. an N-induced low-energy shift of as much as 140 meV occurred. Both the reduction in compressive in-plane strain and the direct effect of N on the bandgap energy contribute to the observed energy shift. Also a PL linewidth broadening by about a factor of five to 32.5 meV, and simultaneously reduced PL peak intensity by a factor of four in comparison to the ternary reference sample, was observed. The integrated intensity, however, remains approximately constant.

Next, $Ga_{0.4}In_{0.6}As_{1-y}N_y$ double-QW structures with $Al_{0.48}In_{0.52}As$ barriers and a well width of 10 nm were grown and analysed. The QW layers were embedded between 100, 30, and 200 nm (in growth direction) thick $Al_{0.48}In_{0.52}As$ barriers lattice matched to the InP substrate, and capped by 5 nm $Ga_{0.47}In_{0.53}As$ to prevent oxidation of the upper barrier. The N concentration in the double-QWs was determined by SIMS depth profiling. The In content

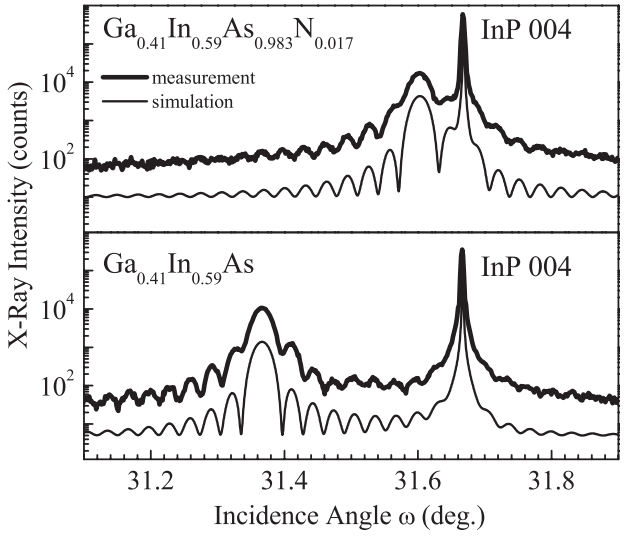

Figure 6. HRXRD profiles of 165 nm thick compressively strained ternary $Ga_{0.41}In_{0.59}As$ and quaternary $Ga_{0.41}In_{0.59}As_{0.983}N_{0.017}$ layer on InP.

was obtained from HRXRD measurements on a ternary $Ga_{1-x}In_xAs$ calibration sample grown under the same condition. The In concentration was $x = 0.60$ and N concentrations were varied in the range $0 \leqslant y \leqslant 0.018$. Figure 8 shows low-temperature (10 K) PL spectra of three double-QW samples with N contents of 0%, 0.8%, and 1.8%. Again, with increasing N concentration the near band edge PL peak shifts to lower energies, accompanied by a peak broadening and a significant reduction in integrated PL intensity [13]. The overall shift of 160 meV for the double-QW structure is comparable to the shift observed for the thick $Ga_{0.41}In_{0.59}As_{1-y}N_y$ films with almost the same In concentrations, as presented above. The difference in absolute peak position of 40 meV is mainly due to quantization effects in the double-QW structure. The FWHM of the double-QWs increased to values of 26 and 70 meV, respectively, with increasing N content. The PL peak intensity was strongly reduced, i.e. by a factor of ten for 0.8% and by more than two orders of magnitude for 1.8% N, respectively, compared to the reference sample.

In figure 9 the experimentally found composition dependence of the $Ga_{0.4}In_{0.6}As_{1-y}N_y$ QW PL peak energy is plotted for the above set of samples (solid squares). To deduce from these data the composition dependence of the gap energy of unstrained bulk-like $Ga_{0.4}In_{0.6}As_{1-y}N_y$, the experimental data have to be corrected numerically for quantization and strain effects. Using calculated values for strain (8.5 meV/% N) and quantization energy (about 50 meV), the corrected data indicated by open triangles are obtained. The largest fraction of the observed PL low-energy shift can thus be attributed to the strong reduction in bandgap energy induced by the incorporation of N. The data points of the 165 nm thick pseudomorphic $Ga_{0.41}In_{0.59}As_{1-y}N_y$ (see figure 7) are also included in figure 9 (crosses), showing good agreement with QW data after the above corrections for strain and quantization. In order to correlate the thus derived $Ga_{0.4}In_{0.6}As_{1-y}N_y$ bandgap energies with room temperature data reported in the literature for $Ga_{1-x}In_xAs_{1-y}N_y$ on GaAs [14, 15], the present data have to be further corrected for the temperature-induced bandgap shift (solid rhombs), taking the same temperature-induced shift of bandgap energy into account as for the ternary $Ga_{0.47}In_{0.53}As$. A comparison with QW PL at 10 and 300 K later in this paper shows an energy shift of about 50 meV (arrow), in reasonable agreement with our assumption. For all these corrections the material parameters of ternary $Ga_{1-x}In_xAs$ have been taken from Serries *et al* [13].

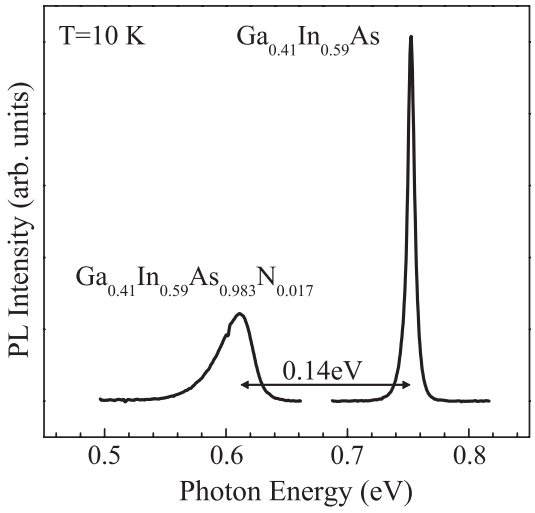

Figure 7. Low-temperature PL spectra of the two samples shown in figure 6: compressively strained $Ga_{0.41}In_{0.59}As$ and $Ga_{0.41}In_{0.59}As_{0.983}N_{0.017}$ on InP.

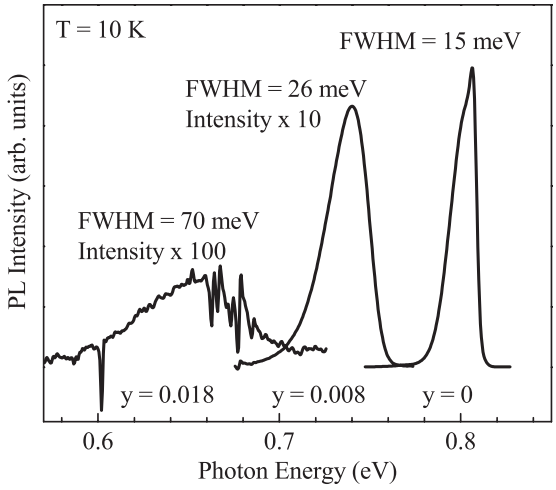

Figure 8. Low-temperature (10 K) PL spectra of a series of 10 nm wide $Ga_{0.40}In_{0.60}As_{1-y}N_y$ double-QWs on InP with various N contents given in the figure.

Taking the valence band discontinuity between GaAs and strained $Ga_{1-x}In_xAs$ as given by Krijn [29], the position of E_N can be computed relative to the conduction band edge of $Ga_{0.4}In_{0.6}As_{1-y}N_y$ on InP assuming that E_N is fixed on an absolute energy scale. Then, the BAC model can be applied to the present set of bandgap data for hypothetic unstrained bulk-like $Ga_{0.4}In_{0.6}As_{1-y}N_y$ using the interaction parameter C_{MN} as a fitting parameter. The resulting fit is shown in figure 9 by the solid line, yielding a value of 2.7 eV for C_{MN}. This value is consistent with $C_{MN} = 2.7$ eV reported for lower In content $Ga_{1-x}In_xAs_{1-y}N_y$ on GaAs [14, 15], thus lending additional support to the BAC model [13].

3.3. The rapid thermal annealing of $Ga_{1-x}In_xAs_{1-y}N_y$ on InP

Post-growth RTA was first applied to the 165 nm $Ga_{0.41}In_{0.59}As_{0.983}N_{0.017}$ film, whose composition and PL was already discussed in section 3.2 (see figures 6, 7). RTA was carried out at 800 °C for 20 s. SIMS yields an N content for the as-grown sample of 1.50%, while for the RTA sample a value of 1.48% is obtained. The difference is within the SIMS accuracy limits of 5% relative change. HRXRD yields an N content of 1.7±0.1% and 1.6±0.1% for the as-grown

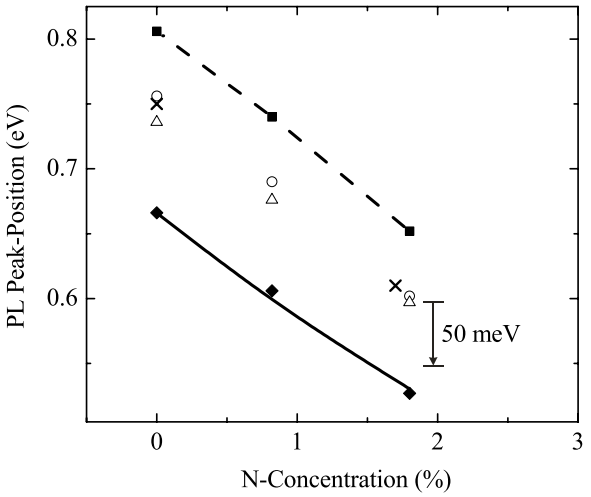

Figure 9. The experimental low-temperature (10 K) peak position (solid squares) for a series of $Ga_{0.40}In_{0.60}As_{1-y}N_y$ double-QWs on InP with varying N content. The dashed curve is drawn to guide the eye. Open circles indicate the bandgap energy of $Ga_{0.40}In_{0.60}As_{1-y}N_y$ corrected for quantization effects, and open triangles represent bandgap energies after correction for strain effects, i.e. they indicate the bandgap energy of unstrained bulk-like $Ga_{0.40}In_{0.60}As_{1-y}N_y$ at 10 K. Solid rhombs show the corresponding bandgap energy corrected for temperature-induced bandgap shift, i.e. at room temperature (300 K). The BAC model fit to the last set of data is shown by the solid curve, yielding the interaction parameter $C_{MN} = 2.7$ eV. Low-temperature PL data points of the 165 nm thick pseudomorphic $Ga_{0.41}In_{0.59}As_{1-y}N_y$ films shown in figure 7 are added (crosses). The temperature-induced energy shift of 50 meV as derived from QW PL at 10 and 300 K (see figure 10) is shown by an arrow.

and RTA sample, respectively, assuming no change in In content during RTA. Thus, with both experimental techniques no change in N content due to RTA was found within the respective accuracy limits. However, we do observe a blueshift of 30 meV in the PL peak position. As can be concluded from the two samples with and without N, PL spectra of which are shown in figure 7, the shift introduced by 1.7% of N amounts to 140 meV, which is 80 meV/% N. Thus for the 30 meV blueshift being solely due to N loss we would expect a reduction in N content from 1.7% to 1.3%, which is a 20% relative change and thus should be detectable with both experimental techniques, SIMS and HRXRD. This implies that other mechanisms, including a rearrangement of III–N bonding, rather than the loss of N are responsible for the observed annealing-induced blueshift in the PL peak position.

In a further step we applied post-growth RTA at 800 °C to a double-QW sample with 60% In and 0.8% N whose PL was discussed in section 3.2. SIMS depth profiles of the QW region of the as-grown sample are shown in figure 10. The Al, Ga, and N signals (upper part of figure 10) appear to be significantly broadened by ion beam induced mixing. The Ga profile of the QW exhibits the typical asymmetrical broadening of the leading and trailing edges. The N profile is broadened in the same way as the Ga profile. For further improvement of the sensitivity, we also analysed the molecular species formed during epitaxy at the interface and due to intermixing during SIMS measurement which is among others Al_2N. Upon annealing we did not observe any change in the Ga and Al signal, as expected, but there was also no change in the N profile and almost no change in the Al_2N signal (lower part of figure 10). For the latter we plotted in figure 10 the Al_2N depth profiles of both the as-grown and annealed material. Only at the leading edges, where the SIMS depth resolution is the highest, can a slight broadening be discerned for the annealed material (indicated by arrows). This observation might be taken

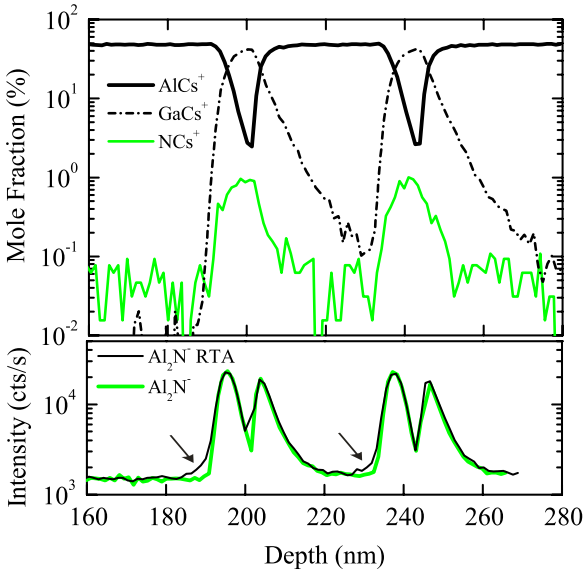

Figure 10. SIMS depth profiles of the QW region of a double-QW structure with $Ga_{0.4}In_{0.6}As_{0.992}N_{0.008}$ QWs and $Al_{0.48}In_{0.52}As$ barriers. The Al, Ga, N (upper part of the figure) and Al_2N (lower part of the figure) signals of the as-grown sample are indicated by bold curves. The result of the RTA sample is plotted only for the most sensitive species Al_2N by a full curve.

as evidence for annealing-induced N diffusion and intermixing; but the observed experimental effect is close to the sensitivity limit.

The low-temperature PL spectra (10 K) of the $Ga_{0.4}In_{0.6}As_{0.992}N_{0.008}$ double-QW sample, subjected to RTA for 20 s at various temperatures, are displayed in figure 11. The PL peak intensity reaches a maximum at 800 °C, which is then nine times the peak intensity of the as-grown sample. Simultaneously the PL peak position is blueshifted by 30 meV. Figure 12 shows both the PL peak energy and FWHM as a function of annealing temperature. For RTA temperatures up to 800 °C the FWHM decreases, whereas the PL peak position is shifted almost linearly towards higher energies. The blueshift is about 25 meV for the sample showing maximum PL intensity (RTA at 800 °C). At 800 °C the minimum FWHM of 15 meV is also reached, which is half the linewidth of the as-grown sample. It can be noted that the maximum PL peak intensity and the minimum linewidth for the $Ga_{0.4}In_{0.6}As_{0.992}N_{0.008}$ double-QW on InP occur at the same RTA temperature of 800 °C. For higher RTA temperatures the sample starts to decompose thermally, indicated by a decreased PL intensity and increased FWHM.

The observed blueshift can be understood in terms of a model assuming that the low-temperature PL is dominated by recombination of excitons trapped at N-induced potential fluctuations. RTA reduces the depth and number of these fluctuations and thus blue-shifts the PL and simultaneously reduces the linewidth [24, 27, 30, 31]. As discussed above for GaInAsN on GaAs, the rearrangement of III–N bonds due to In diffusion [31] or N diffusion [27] may also contribute to the observed annealing effects on the PL spectrum.

3.4. $Ga_{1-x}In_xAs_{1-y}N_y/Al_{1-x}In_xAs$ QW diode lasers on InP

To further explore the long-wavelength limit of pseudomorphic $Ga_{1-x}In_xAs_{1-y}N_y$ QWs on InP, a series of samples consisting of four $Ga_{0.22}In_{0.78}As_{0.99}N_{0.01}$ QWs separated by 30 nm thick lattice matched $Al_{0.48}In_{0.52}As$ barrier layers has been grown and analysed by HRXRD [19]. The QW width was varied between 8 and 14 nm. Low-temperature (10 K) PL spectra of this

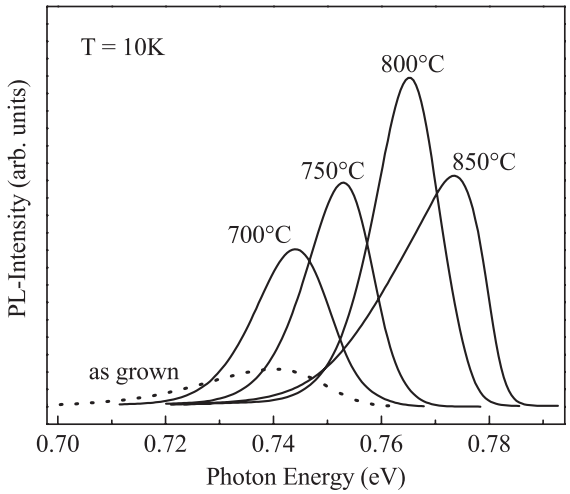

Figure 11. Low-temperature PL spectra (10 K) of the $Ga_{0.4}In_{0.6}As_{0.992}N_{0.008}$ double-QW for different annealing temperatures.

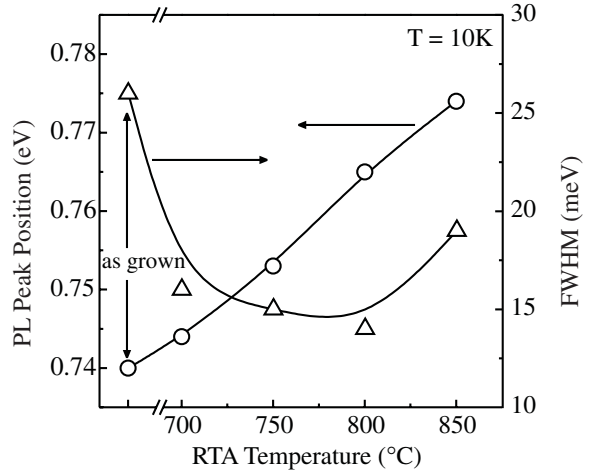

Figure 12. PL energy and linewidth of the $Ga_{0.4}In_{0.6}As_{0.992}N_{0.008}$ double-QW versus RTA temperature. Circles represent the PL energy, squares the linewidth (the curves are a guide to the eye).

series of QW samples are shown in the left-hand panel of figure 13. The PL peak energy decreases, as expected, with increasing well width. The most intense PL signal is observed for the 11 nm wide QWs. A further increase of the QW width to 14 nm leads to a broadening and/or splitting of the PL peak as well as to a reduction of the integrated luminescence intensity, which is characteristic for the onset of strain relaxation. These QW samples showed PL up to at least room temperature, as illustrated in the right-hand panel of figure 13 for the 11 nm wide QWs. There the luminescence signal is peaked at 0.54 eV, corresponding to a 300 K PL wavelength of 2.3 μm. This result demonstrates the potential of highly strained $Ga_{1-x}In_xAs_{1-y}N_y$ QWs for the realization of InP-based 2.3 μm diode lasers.

As the next step, laser structures were grown on sulfur (3–6) $\times$ 10^{18} cm^{-3} doped InP substrates starting with a 30 nm Si-doped lattice matched $Al_{0.15}Ga_{0.32}In_{0.53}As$ buffer followed by an undoped 290 nm $Al_{0.15}Ga_{0.32}In_{0.53}As$ lower separate confinement layer (SCL). Epitaxy continued with three compressively strained $Ga_{0.22}In_{0.78}As_{0.99}N_{0.01}$ QWs separated by 30 nm thick lattice matched $Al_{0.15}Ga_{0.32}In_{0.53}As$ barrier layers. The MBE growth was finished by the upper undoped 290 nm $Al_{0.15}Ga_{0.32}In_{0.53}As$ SCL. Then the wafer was transferred directly into the MOVPE system and overgrown with the upper p-doped InP cladding layer, starting with

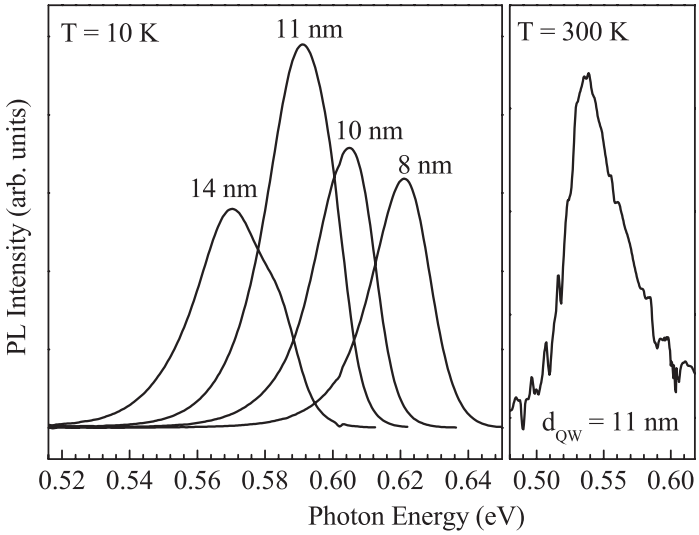

Figure 13. Low-temperature (10 K) PL spectra of $Ga_{0.22}In_{0.78}As_{0.99}N_{0.01}/Al_{0.48}In_{0.52}As$ four-QW samples on InP with different well widths ranging from 8 to 14 nm (left) and room temperature (300 K) PL spectrum of the 11 nm $Ga_{0.22}In_{0.78}As_{0.99}N_{0.01}/Al_{0.48}In_{0.52}As$ four-QW sample showing band-edge luminescence peaked at a wavelength of 2.3 μm (right).

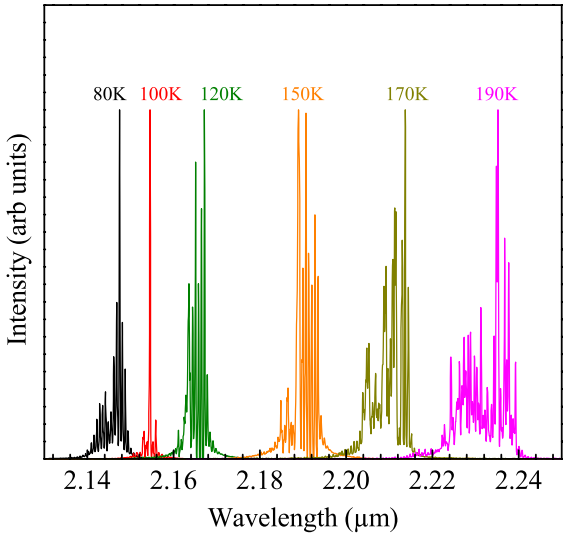

Figure 14. Normalized pulsed lasing spectra recorded with current pulses of 5 μs pulse width and a duty cycle of 5% at various heat sink temperatures of an InP-based $Ga_{0.22}In_{0.78}As_{0.99}N_{0.01}$–MQW ridge waveguide diode laser.

220 nm of undoped InP followed by a 1280 nm thick 1×10^{18} cm^{-3} zinc-doped InP. The laser structure was capped by a 1.1×10^{19} cm^{-3} zinc-doped $Ga_{0.32}In_{0.53}As$ top contact layer. For the first process run the samples were not RTA treated.

Index-guided ridge-waveguide Fabry–Perot lasers were fabricated by standard optical lithography and wet chemical etching. Cleaved laser bars were In-soldered substrate side down on gold-coated copper heat sinks. No facet coating was applied. The laser ridges were electrically contacted by wire bonding to the top p-contact pad. Devices 1750 μm long and 37 μm wide were operated in pulsed mode using current pulses of 5 μs pulse width and a duty cycle of 5%. In figure 14 a sequence of temperature-dependent lasing spectra at a driving

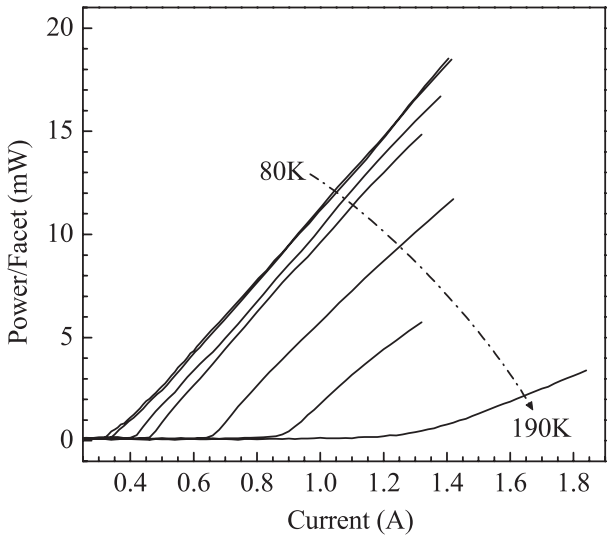

Figure 15. Temperature-dependent light output versus injection current characteristics of an InP-based $Ga_{0.22}In_{0.78}As_{0.99}N_{0.01}$–MQW ridge waveguide diode laser with current pulses of 5 μs pulse width and a duty cycle of 5%.

current just above threshold ($I \approx 1.1I_{th}$) are shown, covering the 80–190 K temperature interval. The lasing wavelength shifts as expected to longer wavelengths, i.e. from 2.15 to 2.23 μm with increasing temperature. Temperature-dependent output power-versus-current characteristics taken from the same device are plotted in figure 15. While at low temperatures output powers of several tens of milliwatts are readily achieved, the threshold current increases and the slope efficiency decreases rapidly with increasing heat sink temperature. Thus, the maximum operating temperature using 5 μs long current pulses is limited to slightly below 200 K. The poor high-temperature performance so far, reflected by a threshold current density of close to 2 kA cm^{-2} at maximum operating temperature, is attributed to the poor $Ga_{0.22}In_{0.78}As_{0.99}N_{0.01}$ material quality. Reference lasers containing N-free $Ga_{0.22}In_{0.78}As$ QWs as the active region, which emit at around 1.9 μm, show a factor of 30 lower threshold current density at 200 K. It should be noted that no post-growth annealing was applied to the $Ga_{0.22}In_{0.78}As_{0.99}N_{0.01}$ laser structures. However, as shown above, for $Ga_{0.4}In_{0.6}As_{0.992}N_{0.008}$ QWs on InP optimized post-growth annealing also results in a significant improvement in $Ga_{0.4}In_{0.6}As_{0.992}N_{0.008}$ luminescence properties. Therefore, applying post-growth 800 °C RTA to the present InP-based $Ga_{0.22}In_{0.78}As_{0.99}N_{0.01}$ QW laser material should result in a significant reduction in threshold current and thus enable room temperature operation with an emission wavelength around 2.3 μm.

4. Conclusion

In summary, we have shown the feasibility of high In-containing III–AsN structures and demonstrated the possibility to achieve wavelengths beyond 2 μm using InP-based pseudomorphic $Ga_{1-x}In_xAs_{1-y}N_y$ QWs. Post-growth thermal annealing improves the material quality also for the high In-containing QW structures on InP. Finally we demonstrated a $Ga_{0.22}In_{0.78}As_{0.99}N_{0.01}$–MQW laser on InP.

Acknowledgments

The authors would like to thank N Rollbühler for performing the MOVPE overgrowth, T Fuchs for expert assistance in the SIMS analyses, H Güllich and F Windscheid for carrying out the HRXRD measurements as well as M Kunzer for the PL measurements. Continuous interest

and encouragement by G Weimann is gratefully acknowledged. Part of the work was supported by the German Ministry for Education and Research.

References

[1] Kondow M, Uomi K, Niwa A, Kitatani T, Watahiki S and Yazawa Y 1996 *Japan. J. Appl. Phys.* 1 **35** 1273
[2] Kurtz S R, Allermann A A, Jones E D, Gee J M, Banas J J and Hammons B E 1999 *Appl. Phys. Lett.* **74** 729
[3] Héroux J B, Yang X and Wang W I 1999 *Appl. Phys. Lett.* **75** 2716
[4] Bi W G and Tu C W 1997 *Appl. Phys. Lett.* **70** 1608
[5] Bellaiche L, Wei S-H and Zunger A 1997 *Appl. Phys. Lett.* **70** 3558
[6] See e.g., Vurgaftman I, Meyer J R and Ram-Mohan L R 2001 *J. Appl. Phys.* **89** 5815
[7] Kondow M, Kitatani T, Nakahara K and Tanaka T 1999 *Japan. J. Appl. Phys.* 2 **38** L1355
[8] Egorov A Yu, Bernklau D, Livshits D, Ustinov V, Alferov Zh I and Riechert H 1999 *Electron. Lett.* **35** 1643
[9] 2002 *Semicond. Sci. Technol.* **17** (8) (Special issue: III–V–N Semiconductor Alloys)
[10] Gokhale M R, Wei J, Wang H and Forrest S R 1999 *Appl. Phys. Lett.* **74** 1287
[11] Bellaiche L 1999 *Appl. Phys. Lett.* **75** 2578
[12] Ubukata A, Dong J, Matsumoto K and Ishihara Y 2000 *Japan. J. Appl. Phys.* 1 **39** 5962
[13] Serries D, Geppert T, Ganser P, Maier M, Köhler K, Herres N and Wagner J 2002 *Appl. Phys. Lett.* **80** 2448
[14] Shan W, Walukiewicz W, Ager J W III, Haller E E, Geisz J F, Friedman D J, Olson J M and Kurtz S R 1999 *Phys. Rev. Lett.* **82** 1221
[15] Shan W, Walukiewicz W, Yu K M, Ager J W III, Haller E E, Geisz J F, Friedman D J, Olson J M, Kurtz S R and Nauka C 2000 *Phys. Rev.* B **62** 4211
[16] Maier M, Serries D, Geppert T, Köhler K, Güllich H and Herres N 2003 *Appl. Surf. Sci.* **203/204** 486
[17] Wagner J, Köhler K, Ganser P and Herres N 2000 *Appl. Phys. Lett.* **77** 3592
[18] Wagner J, Geppert T, Köhler K, Ganser P and Herres N 2001 *J. Appl. Phys.* **90** 5027
[19] Serries D, Geppert T, Köhler K, Ganser P and Wagner J 2003 *Mater. Res. Symp. Proc.* **744** 627
[20] Buyanova I A, Chen W M, Pozina G, Bergman J P, Monemar B, Xin H P and Tu C W 1999 *Appl. Phys. Lett.* **75** 501
[21] Buyanova I A, Pozina G, Hai P N, Tinh N Q, Bergman J P, Chen W M, Xin H P and Tu C W 2000 *Appl. Phys. Lett.* **77** 2325
[22] Alt H Ch, Egorov A Yu, Riechert H, Wiedemann B, Meyer J D, Michelmann R W and Bethge K 2000 *Appl. Phys. Lett.* **77** 3331
[23] Kurtz S, Webb J, Gedvilas L, Friedman D, Geisz J, Olson J, King R, Joslin D and Karam N 2001 *Appl. Phys. Lett.* **78** 748
[24] Geppert T, Wagner J, Köhler K, Ganser P and Maier M 2002 *Appl. Phys. Lett.* **80** 2081
[25] Harrison W A 1980 *Electronic Structure and the Properties of Solids* (San Francisco, CA: Freeman) p 176
[26] Kim K and Zunger A 2001 *Phys. Rev. Lett.* **86** 2609
[27] Klar P J, Grüning H, Koch J, Schäfer S, Volz K, Stolz W, Heimbrodt W, Kamal Saadi A M, Lindsay A and O'Reilly E P 2001 *Phys. Rev.* B **64** 121203
[28] Herres N, Kirste L, Obloh H, Köhler K, Wagner J and Koidl P 2002 *Mater. Sci. Eng.* B **91/92** 425
[29] Krijn M P C M 1991 *Semicond. Sci. Technol.* **6** 27
[30] Tournié E, Pinault M-A and Guzmán A 2002 *Appl. Phys. Lett.* **80** 4148
[31] Albrecht M, Grillo V, Remmele T, Strunk H P, Egorov A Yu, Dumitras Gh, Riechert H, Kaschner A, Heitz R and Hoffmann A 2002 *Appl. Phys. Lett.* **81** 2719